Mean-field coefficients for helical flow fields

GIESECKE A., STEFANI F., GERBETH G.
Helmholtz-Zentrum Dresden-Rossendorf, P.O. Box 510119, D-01314 Dresden – Germany
e-mail: a.giesecke@hzdr.de

Abstract: We perform simulations of the kinematic induction equation in order to examine a helical flow of a conducting liquid interacting with magnetic material with permeability $\mu > 1$. We examine two paradigmatic systems that reflect the flow conditions in the core of a sodium fast reactor, and we show that in the limit of large μ the critical magnetic Reynolds number required for the onset of dynamo action is reduced by 25%.

1. Introduction

The experimental confirmation of the magnetohydrodynamic dynamo effect has been of great importance for the understanding of geo- and astrophysical magnetic fields. Besides of this fundamental relevance, a complementary argument for the development of dynamo experiments originated from considerations on the safe operation of sodium fast reactors [1] because the helical structure of the flow in the core (figure 1), combined with the large flow rate, provides appropriate prerequisites for the occurrence of dynamo action. However, this effect is undesired, because the backreaction of a self-excited magnetic field may cause an inhomogeneous flow braking or a pressure drop in the cooling system, so that an efficient removement of heat from the reactor core can be hampered with unknown consequences for the safety of the reactor.

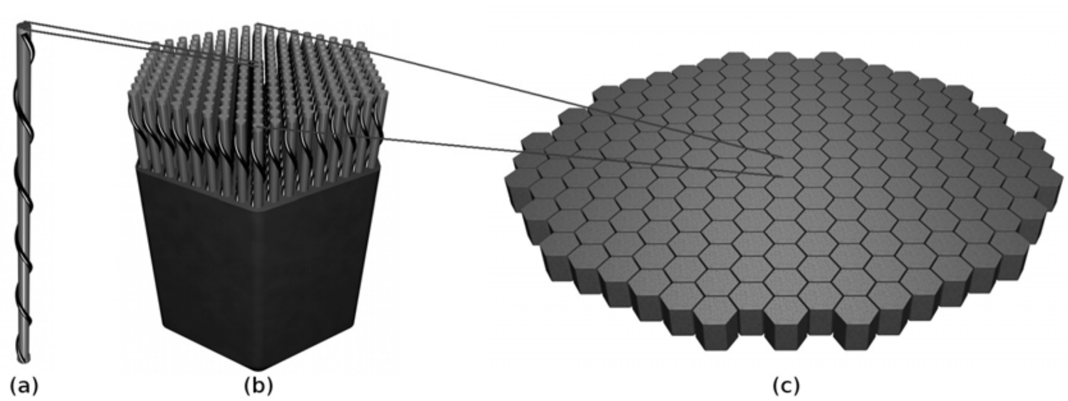

Figure 1: Idealized composition of the core of a sodium fast reactor. (a) Nuclear fuel rod surrounded by a screw-like spacer that forces the flow on a helical path. (b) A few hundreds of fuel rods are bundled into so-called assemblies. (c) The whole reactor core is composed of a few hundreds of assemblies.

Previous studies have shown no conclusive evidences for the occurrence of dynamo action in the core of a fast reactor [2,3,4,5], but it is hypothesized that the parameter regime reached by the French fast breeder reactor *Superphenix* is well within the range that allows for dynamo action if some magnetic material is introduced into the core [6]. In the present study we revisite the arguments from [6], and in order to develop global models for electromagnetic induction in the core of fast reactors we resort to the mean-field dynamo theory [7] which allows a consideration of tens of thousands of helical flow cells in terms of an α- and β-effect including the impact of magnetic material. We develop and validate the necessary methodology required for the computation of the mean-field coefficients which may be used for future estimates of dynamo action in systems that are characterized by different size and different magnetic materials. The examination of the impact of magnetic material is motivated by the key role of soft iron impellers for the VKS dynamo and by the repeatedly manifested idea to make use of *Oxide Dispersion Strengthened* (ODS) ferritic/martensitic alloys in the core of a fast reactor. These alloys have a lower sensitivity for nuclear radiation, but exhibit a permeability much larger than one. We start with the analysis of the induction action of the fully resolved velocity field and compute the mean-field coefficients required for a consistent mean-field model using the testfield method [8]. In a second step we use the α- and β-coefficients as an input for mean-field dynamo simulations in order to proof that mean-field models are capable to reproduce the growth-rate and principle field structure of the fully resolved model by requiring much less computational efforts.

2. Mean-field dynamo theory and testfield method

We splitt the magnetic field and the velocity field into a mean, large scale part and a small scale part: $\mathbf{B} = \overline{\mathbf{B}} + \mathbf{b}$ and $\mathbf{U} = \overline{\mathbf{U}} + \mathbf{u}$. Then the mean magnetic field is governed by the mean field induction eqaution:

$$\partial\overline{\mathbf{B}} / \partial t = \nabla \times \left(\overline{\mathbf{U}} \times \overline{\mathbf{B}} + \overline{\mathbf{u} \times \mathbf{b}} - \eta \nabla \times \overline{\mathbf{B}}\right) \tag{1}$$

which includes a term called the mean electromotive force $\mathbf{F} = \overline{\mathbf{u} \times \mathbf{b}}$, which only depends on the statistical properties of small scale flow and small scale field. Under the assumptions that the variations of $\overline{\mathbf{B}}$ around a given point are small, $\mathbf{F}$ can be represented by the first terms of a Taylor expansion

$$F_i = \alpha_{ij}\overline{B}_j + \beta_{ijk}\partial\overline{B}_j / \partial x_k. \tag{2}$$

In order to compute the mean-field coefficients we utilize the testfield method developped by Schrinner et al [8]. In that method α_{ij} and β_{ijk} are computed from different realizations of the electromotive force that are obtained from externally applied, linearly independent mean fields. Defining the small scale velocity as the deviation from the horizontal average, the small scale magnetic field is computed numerically by solving

$$\partial\mathbf{b} / \partial t = \nabla \times \left(\overline{\mathbf{U}} \times \mathbf{b} + \mathbf{u} \times \overline{\mathbf{B}} + \left(\mathbf{u} \times \mathbf{b} - \overline{\mathbf{u} \times \mathbf{b}}\right) - \eta \nabla \times \mathbf{b}\right). \tag{3}$$

Then the electromotive force is computed directly by correlating small scale flow with the small scale field and subsequently performing a horizontal averaging. The combination of different realizations of $\mathbf{F}$ obtained from different, linearly independent testfields yields a linear system of equations, whose solution gives the desired mean-field coefficients. In order to compute mean-field coefficients that are consistent with the structure of the large scale field from the fully resolved model, it is necessary to consider the scale dependence of the mean-field coefficients by choosing appropriate testfields. We define the testfields as follows:

$$\overline{\mathbf{B}}_1 = \cos(\pi z)\hat{\mathbf{y}} \text{ and } \overline{\mathbf{B}}_2 = \sin(\pi z)\hat{\mathbf{y}} \tag{4}$$

which is in agreement with the definitions used by [10].

3. Flow model and permeability distribution

In the present study we examine two paradigmatic flow models: In model A we assume a flow consisting of various helical eddies that are separated by walls (left panel in figure 3). Following the idea of [3], the helical flow within one cell represents the mean flow within one assembly of nuclear fuel rods ignoring the even smaller scale flow around individual rods. The second approach (model B, see right panel in figure 4) uses a more detailed picture of the

flow conditions within a single assembly. The model is based on the so called spin generator flow that has been utilized for the simulation of the Karlsruhe Dynamo [9] and assumes a circular flow around a central rod superimposed with a constant vertical flow.
In order to characterize the amplitude of the flow we define a local magnetic Reynolds number that is based on the flow amplitude u_0, the "normal" magnetic diffusivity $\eta = (\mu_0\sigma)^{-1}$ and the size D of a single eddy (model A) or the distance between two adjacent rods (model B): $Rm = u_0 D / \eta$.

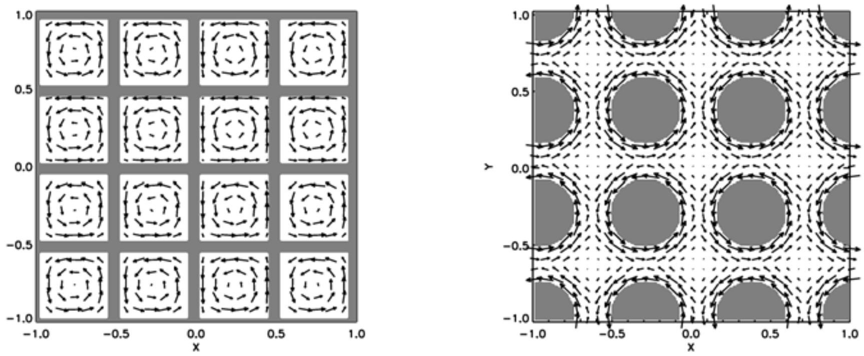

Figure 2: Flow pattern for model A (left) and model B (right). The gray shaded regions represent walls or rods and may have a permea-bility $\mu_r > 1$. The vertical flow is constant in each cell and vanishes in the wall/rod regions. The horizontal flow is denoted by the arrows.

In order to incorporate the effects of a non-uniform permeability distribution in terms of mean-field coefficients we rewrite the induction equation in the form

$$\partial \mathbf{B} / \partial t = \nabla \times \left(\mathbf{U} \times \mathbf{B} + \eta \nabla \ln \mu_r \times \mathbf{B} - \eta \nabla \times \mathbf{B}\right) \qquad (6)$$

with $\eta = \eta / \mu_r(r)$. This modified induction equation contains an additional velocity-like term $u(r) = \eta \nabla \ln(\mu_r)$ which contributes to the mean flow as well as to the small scale flow when applied in the testfield method.

4. Results

The results for a uniform permeability distribution with $\mu_r = 1$ are shown in figure 3. The α-effect is in accordance with the results reported by [9] in case of the ideal Roberts flow. In the same way we write $\alpha = K\eta / DRm^2 \Phi(Rm)$ with a non-analytic function Φ that only depends on Rm and a normalisation factor K that is universal for each model and does not depend on the cell size D. Regarding the coefficient β we find significant differences between both models. In model A we see a transition to negative values (but in a way that the sum of η and β remains positive), whereas the β-effect remains allways positive in model B. The right column in figure 3 shows a comparison of the growth-rates from the fully resolved models (FRM) with the corresponding mean field models (MFM) that made use of the coefficients determined from the FRM. The mean field induction equation that is solved numerically reads

$$\partial \overline{\mathbf{B}} / \partial t = \nabla \times \left(\overline{\mathbf{U}} \times \overline{\mathbf{B}} - \alpha\left(\overline{\mathbf{B}} - \gamma \hat{\mathbf{z}} \times \overline{\mathbf{B}} - (\hat{\mathbf{z}} \cdot \overline{\mathbf{B}})\hat{\mathbf{z}}\right) - \bar{\eta} \nabla \times \overline{\mathbf{B}} - \beta \hat{\mathbf{z}} \times d\overline{\mathbf{B}} / dz - \delta_2 (\hat{\mathbf{z}} \cdot \nabla)\overline{\mathbf{B}}\right) \qquad (7)$$

where the coefficients α, β, γ and δ_2 are related to the tensor elements from Eq. (2) by $-\alpha = \alpha_{xx} = \alpha_{yy}$, $\beta = \beta_{xyz} = -\beta_{yxz}$, $-\gamma = \alpha_{xy} = -\alpha_{yx}$ and $\delta_2 = \beta_{xxz} = \beta_{yyz}$.
We obtain a good agreement between FRM and MFM if the system is not strongly over-critical. The agreement improves for an increasing number of helical eddies. However, the

results become more complex when $\mu_r > 1$ (figure 4). For a fixed μ_r we always find that α grows

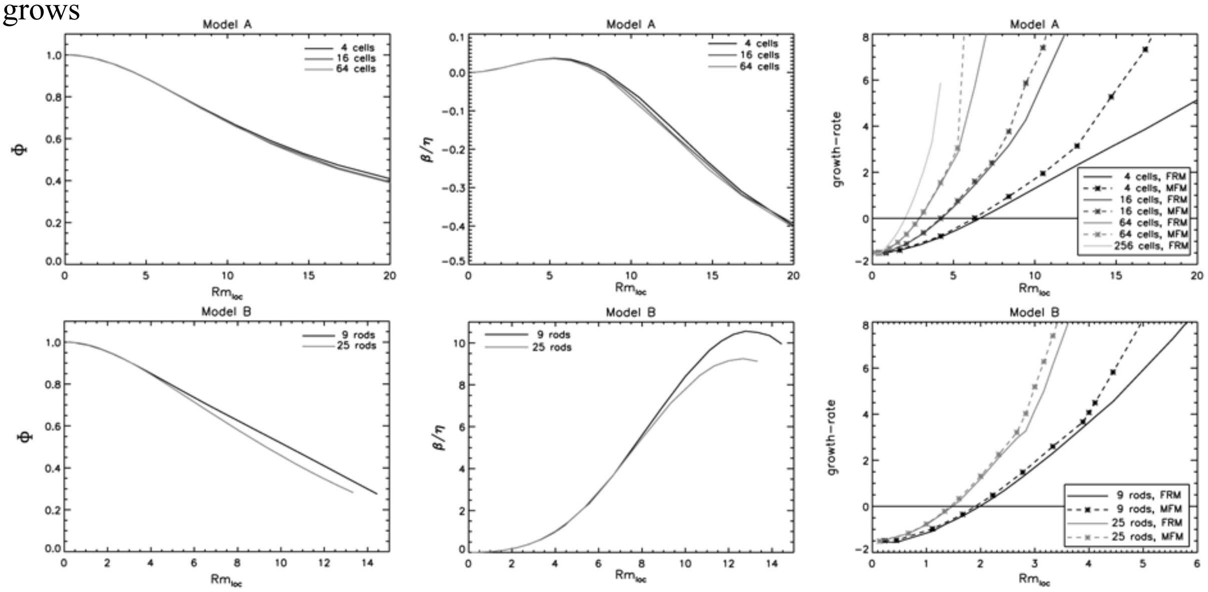

Figure 3: Mean field coefficients and growth-rates versus Rm for μ_r=1. From left to right: Φ, β, and growth-rates. Solid curves denote the growth-rates from the fully resolved model (FRM) and dashed curves denote the growth-rates from the mean-field models (MFM). Top row: model A, bottom row: model B.

with increasing *Rm*. Both models show a different behavior concerning the dependence on μ_r. For model A, we observe a significant supression of α for small μ_r, followed by a slow recovery for larger μ_r. In contrast, we see a moderate increase of α for small μ_r in model B followed by a saturation regime for μ_r>1.

Regarding the coefficient β, we find an abrupt transition to negative values around $\mu_r \approx 3$ in model A, whereas β increases linearly with increasing μ_r in model B, which, furthermore, does not show any indications for a transition to negative values.

Again, we find a good agreement between the FRM growth-rates and the MFM growth-rates but with some increasing deviations for large *Rm* and large μ_r. Considering the whole range of achievable μ_r in model A we find a reduction of the critical magnetic Reynolds number from Rm^{crit} = 4.2 at μ_r = 1 to Rm^{crit} = 3.2 at μ_r = 20. The relative reduction is roughly the same for

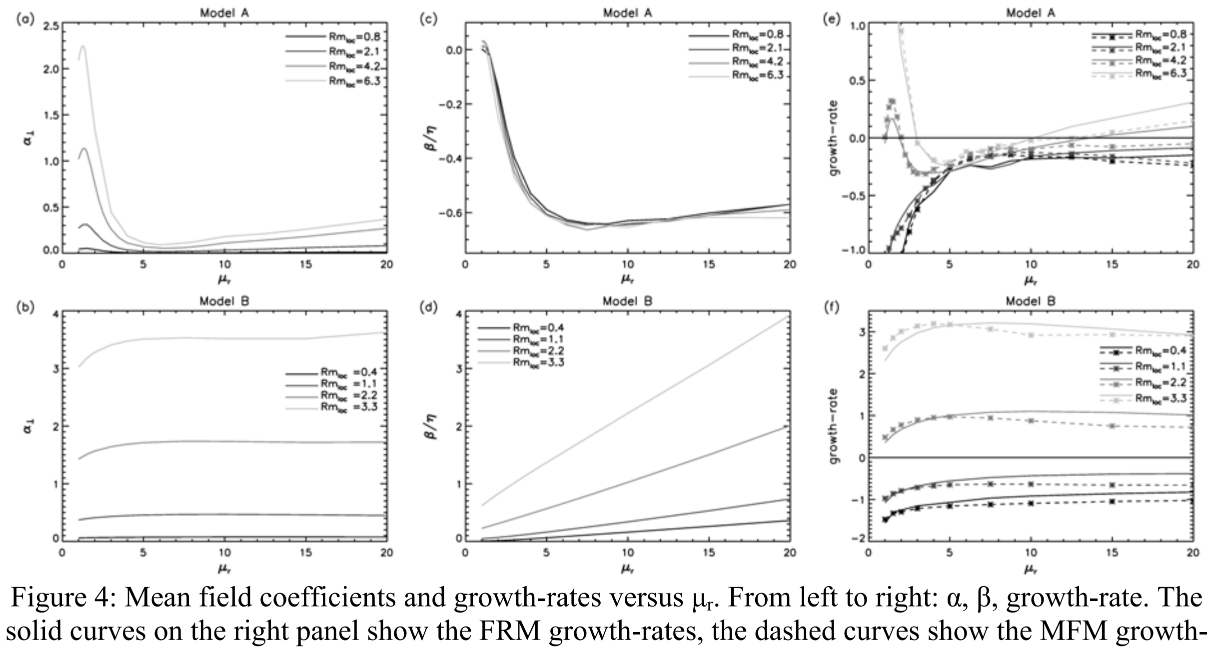

Figure 4: Mean field coefficients and growth-rates versus μ_r. From left to right: α, β, growth-rate. The solid curves on the right panel show the FRM growth-rates, the dashed curves show the MFM growth-rates. Top row: model A, bottom row: model B.

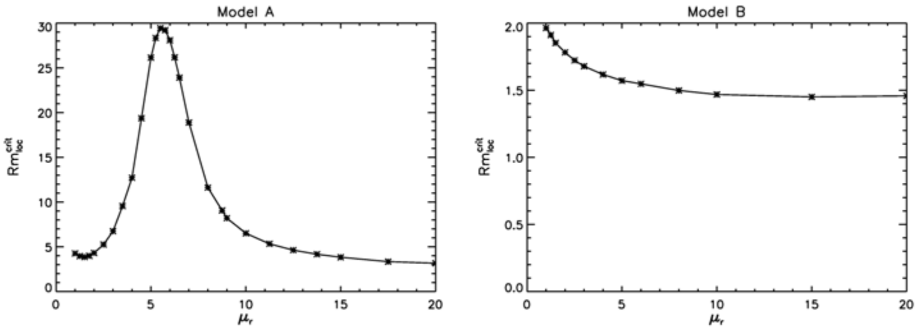

Figure 5: Critical magnetic Reynolds number for the onset of dynamo action versus permeability. Left: model A, right: model B.

model B, where $Rm^{\mathrm{crit}} = 2.0$ at $\mu_{\mathrm{r}}=1$ is reduced to $Rm^{\mathrm{crit}} = 1.5$ at $\mu_{\mathrm{r}} = 20$ (figure 5). Regarding the asymptotic behavior for large μ_{r} in figure 5 it seems unlikely that a further increase of μ_{r} will provide for a further significant reduction of Rm^{crit}.

5. Conclusion

We have performed numerical simulations of the kinematic induction equation for two different helical flow types including internal walls or rods that may have magnetic properties. In the limit of large permeability, we found a moderate impact of μ_{r} on dynamo action in terms of a reduction of Rm^{crit} of roughly 25% compared to the non-magnetic case.
Comparing the growth-rates obtained from fully resolved models with the corresponding mean-field models we found a good agreement between both approaches, at least for $\mu_{\mathrm{r}} < 20$.
For non-magnetic internals we show that the α-effect can be expressed in terms of a function Φ that allows a conclusion on α for larger systems when flow scale and flow amplitude are known. In combination with the β-effect, which is roughly independent of the flow scale, this allows a modelling of systems that may consist of tens of thousands of individual helical cells embedded into some large scale flow structure.
The possible application to specific reactor cores will need much more information on geometric details and material properties, such as the size of the core, the number of fuel rods contained therein, and the total flow rate as well as the consideration of the hexagonal geometry of the assemblies, which will be left for future work. Nevertheless, we believe that a consideration of these details will only result in minor modifications to our findings and are therefore of secondary importance.

Acknowledgements. The authors kindly acknowledge support by the Helmholtz Allianz LIMTECH.

References

[1] Rädler, K. H. in 'Magnetohydrodynamics - Historical Evolution and Trends', Springer (2007), 55-72.
[2] Bevir, M. K.: J. Brit. Nucl. Eng. Soc. 12 (1973), 455-458.
[3] Pierson, E. J.: Nucl. Sci. Eng. 57 (1975), 155-163.
[4] Plunian, F., Marty, P., Alemanny, A.: J. Fluid Mech. 382 (1999), 137-154.
[5] Alemany, A., Marty, P., Plunian, F. & Soto, J.: J. Fluid Mech. 403 (2000), 263-276.
[6] Soto, J.: PhD thesis, L'Institut National Polytechniques De Grenoble (1999).
[7] Krause, F. & Rädler, K. H.: Mean-field magnetohydrodynamics and dynamo theory, Pergamon Press 1980.
[8] Schrinner, M. et al.: Astron. Nachr. 326 (2005), 245-249.
[9] Rädler, K. H. et al.: Nonlin. Processes Geophys. 9 (2002), 171-187.
[10] Rädler, K. H. & Brandenburg, A.: Phys. Rev. E 67 (2003), 026401.